



Adsorption studies of an azo dye using polyaniline coated calcined layered double hydroxides

Sousna Sahnoun^a, Mokhtar Boutahala^{a,*}, Gisèle Finqueneisel^b, Thierry Zimny^b, Abdelkrim Kahoul^c

^aLaboratoire de Génie des Procédés Chimiques (LGPC), Département de Génie des Procédés, Faculté de Technologie, Université Ferhat Abbas, Sétif-1-19000, Algeria, emails: mboutahala@yahoo.fr (M. Boutahala), ssnsahnoun@yahoo.fr (S. Sahnoun)

^bLaboratoire de Chimie et Physique Approche Multi-échelle des Milieux Complexes (LCPA2MC), 57500 Saint-Avold, France, emails: gisele.finqueneisel@univ-lorraine.fr (G. Finqueneisel), thierry.zimny@univ-lorraine.fr (T. Zimny)

^cLaboratoire d'Énergétique et d'Electrochimie du solide (LEES), Département de Génie des Procédés, Faculté de Technologie, Université Ferhat Abbas, Sétif-1, 19000 Sétif, Algérie, email: kahoulabdelkrim@yahoo.fr

Received 11 September 2017; Accepted 12 July 2018

ABSTRACT

In this study, novel composite polyaniline/calcined layered double hydroxides was synthesized through the chemical method using the ammonium persulfate as an oxidant and investigated for its behavior in selective and high adsorption of tartrazine dye from an aqueous solution in a batch system. Scanning electron microscope, Fourier transform infrared spectroscopy, X-ray diffraction, Brunauer–Emmett–Teller method and thermogravimetric analysis were carried out. The effects of solution pH, initial concentration and contact time were investigated. The adsorption processes show that the maximum adsorption capacity of tartrazine was 487.8 mg/g, obtained for the MgAlC-PANI composite and well fitted to Langmuir isotherm model. The adsorption processes followed the pseudo-second-order kinetics model with a very high correlation coefficient of $0.998 < R^2 < 1$. The regeneration studies revealed that the tartrazine loaded MgAlC-PANI could be reused for four consecutive cycles.

Keywords: Polyaniline; Hydrotalcite; Calcination; Composite; Azo dye; Adsorption

1. Introduction

Dye adsorption from aqueous solutions is of great practical attention in the context of wastewater treatment because the dyes are considered as priority contaminants due to their low biodegradability, stability and toxicological profile [1]. In addition, most of these dyes have a recalcitrant and inhibitory nature because of their large size and complex molecular structures and are thus considered non-oxidizable by conventional physical and biological treatments [2]. In particular, azo dyes and their derivatives are mutagenic and carcinogenic, posing serious dangers to human health and aquatic life [3]. They facilitate introduction into the body by ingestion and

damage the DNA [4]. One of the major sources of water pollution is wastewater containing dyes so they must be treated before discharge to the natural water bodies [5]. Various chemical, physical and biological methods for dye removal have been developed. One of these methods is adsorption which is an advantageous technique because of its simplicity of design, availability of adsorbents and low cost [6–9].

Many adsorbents have been used to remove azo dye ions from aqueous solutions, for examples, sepiolite clay [10], p-tert-butylcalixarene immobilized material [11], activated carbon derived from “waste” bamboo culms [12], humics-modified silica gel [13], diatomite/chitosan-Fe (III) composite [14], nanodiamond surface [15] and layered double hydroxides (LDHs) [16,17].

* Corresponding author.

LDHs or hydrotalcite-like compounds are composed of positively charged brucite-like sheets and negatively charged anions in the hydrated interlayer regions. Their general formula is $[M_{1-x}^{II}M_x^{III}(\text{OH})_2]^{x+} (A^{n-})_{x/n} \cdot m\text{H}_2\text{O}$, where M^{II} and M^{III} are divalent metal cations (Mg^{2+} , Zn^{2+} , Ni^{2+} , Cu^{2+} , Ca^{2+} , etc.) and trivalent metal cations (Al^{3+} , Fe^{3+} , Ga^{3+} , Cr^{3+} , etc.), respectively. A^{n-} denotes an exchangeable interlayer anion with a negative charge n , m is the number of water interlayers and x is defined as the $M^{III}/(M^{II} + M^{III})$ ratio [18].

The calcination of these LDHs (CLDHs) produces non-stoichiometric mixed metal oxides as intermediates and provides high specific surface areas, high anion exchange capacities, strong Lewis basic sites, flexible interlayer space and homogeneous dispersion of metal cations [19]. Rehydration of CLDHs leads to the rebuilding of the original layered structure, which is called the “memory effect” [20]. As a kind of promising adsorbents, CLDHs have been widely used for the removal of contaminant anions in wastewaters, even better than their LDH precursors [16,17].

In the last two decades, conducting polymers have been of particular interest due to their potential applications in areas such as anti-corrosion, coatings, batteries, sensors, electrochromic displays, microelectronics, super capacitors and diodes. Among all the conducting polymers, polyaniline (PANI) is one of the most important conducting polymers because of its easy preparation, high electrical conductivity, environmental stability and cost-effectiveness [21]. The emeraldine salt (ES) form of PANI appears to be polycationic and may provide a cationic site for adsorption of the anion, and the existence of the amino and imine groups in the backbones may be in favor of the adsorption as well [22].

Composites of polyaniline along with clay have been prepared and used as an adsorbent. In literature, beidellite [23], zeolite [24], attapulgite [25,26], montmorillonite [27,28], palygorskite [29] were coated by polyaniline for the removal of pollutants from wastewater. These composites lead to produce an effective adsorbent because there are plenty of amine and imine groups in polyaniline, which can adsorb the anionic dye species through electrostatic interactions or hydrogen bonds [30].

In this study, MgAlC-PANI composite was synthesized by an in situ chemical polymerization method using APS (ammonium peroxydisulfate) as an oxidant and characterized by scanning electron microscopy (SEM), X-ray diffraction (XRD), Fourier transform infrared spectroscopy (FTIR), Brunauer-Emmett-Teller (BET) and thermogravimetric analysis (TGA) techniques. The capacity for the removal of an azo dye was analyzed and the effect of different parameters including pH of solution, reaction time and initial concentration of the dye on the removal efficiency was investigated in detail. Adsorption kinetics and adsorptions isotherms were also examined. To the best of our knowledge, there is no any report devoted to the potential applicability of PANI with calcined magnesium aluminum layered double hydroxide MgAlC for the removal of an azo dye from an aqueous solution.

2. Experimental setup

2.1. Materials

All chemicals used in the synthesis of magnesium layered double hydroxides such as $\text{MgCl}_2 \cdot 6\text{H}_2\text{O}$, $\text{AlCl}_3 \cdot 9\text{H}_2\text{O}$, Na_2CO_3 ,

NaOH were purchased from Sigma-Aldrich (France). Aniline (ANI) and ammonium persulfate required for the polymer were obtained from GPR RECTAPUR (Merck, France). Tartrazine (TAR), shown in the inset of Fig. 7, is an anionic dye (4,5-dihydro-5-oxo-1-(4-sulfophenyl)-4-[(4-sulfophenyl) azo]-1H pyrazole-3-carboxylic acid trisodium salt), also known as Acid Yellow 23, with a molecular weight 534.4 and a molecular formula $\text{C}_{16}\text{H}_9\text{N}_4\text{Na}_3\text{O}_9\text{S}_2$, was also purchased from Sigma-Aldrich. All materials were used as received without purification.

2.2. Preparation of the adsorbents

2.2.1. Synthesis of MgAl- CO_3 and MgAlC

The layered double hydroxide MgAl- CO_3 with $[\text{Mg}]/[\text{Al}]$ ratio equal to 2 was synthesized by co-precipitation at a constant pH of 10 following the method described by Reichle et al. [18]. A mixed solution of 0.66 mol of $\text{MgCl}_2 \cdot 6\text{H}_2\text{O}$ and 0.33 mol of $\text{AlCl}_3 \cdot 9\text{H}_2\text{O}$ in 500 mL of distilled water was added dropwise under vigorous stirring to 500 mL of an aqueous solution containing 2 mol of NaOH and 1 mol of Na_2CO_3 . During the co-precipitation process, the pH was maintained at 10 by addition of 1 N HNO_3 solution. The obtained gel was stirred for 18 h at 70°C until crystallization. The solid was filtered and washed with distilled water until obtaining a Cl^- free MgAl- CO_3 using AgNO_3 test. This material was then dried at 80°C for 24 h, ground and finally stored in plastic bottles. A fraction of the resulting material was calcined at 500°C for 4 h. The solid obtained was noted MgAlC.

2.2.2. Synthesis of polyaniline

The synthesis method described below is a modification of the procedure described by Sun et al. [31]. The pure polyaniline was synthesized by oxidative polymerization of aniline monomer using sodium persulfate as an oxidizing agent in hydrochloric acid solution. The mixture was magnetically stirred for 4 h. Then, the greenish-black solid material obtained (PANI) was washed with distilled water until no free Cl^- ion was detected in the filtrate. Finally, the PANI powder was dried at 60°C.

2.2.3. Synthesis of MgAlC-PANI

MgAlC-PANI was synthesized by oxidative polymerization. In detail, an amount of MgAlC was dispersed in HCl solution. Then 1 mL of aniline was added into the suspension. A known amount of ammonium persulfate solution was then added dropwise to the suspension within 4 h under mechanical stirring. The sample was centrifuged and washed several times with distilled water until no free Cl^- ions stop appearing in the filtrate and then dried at 60°C.

2.3. Dye adsorption experiments

The adsorption of TAR was conducted in batch experiments. Aqueous solutions of certain concentrations of adsorbate were studied by using 10 mL of the dye solution and 10 mg of adsorbent under agitation. The supernatant liquid was centrifuged out and the equilibrium concentration of TAR was determined using UV-Vis spectra (Shimadzu

UV-1700 UV/VIS spectrophotometer) at 426 nm. The effect of various parameters: initial TAR concentration, pH, contact time on TAR uptake was investigated. The removal (%) of tartrazine and the amounts adsorbed onto the adsorbent at equilibrium q_e (mg/g) and at any time q_t (mg/g) were calculated using the following relationships:

$$R(\%) = \frac{C_0 - C_e}{C_0} \times 100 \quad (1)$$

$$q_{e,t} = \frac{(C_0 - C_{e,t}) \cdot V}{m} \quad (2)$$

where $q_{e,t}$ (mg/g) is the amount of adsorbed tartrazine at equilibrium (q_e) or at any time (q_t); V is the volume of solution (L), C_0 (mg/L) is the initial dye concentration; $C_{e,t}$ is the tartrazine concentrations at equilibrium (C_e) or at any time (C_t) (mg/L) and m is the weight (g) of the adsorbent.

2.4. Analysis of the data

The values of the kinetic and isotherm parameters were determined by a linear regression analysis using ORIGIN program (version 8.5). The linear correlation coefficients (R^2) were used to analyse the data set to confirm the best fit for kinetics and isotherm models for the adsorption. If data from the models are similar to those obtained in experiments, the R^2 will be close to 1. It was evaluated using Eq. (3) as follows:

$$R^2 = 1 - \frac{\sum_{n=1}^n (q_{e,t,\text{exp},n} - q_{e,t,\text{cal},n})^2}{\sum_{n=1}^n (q_{e,t,\text{exp},n} - \overline{q_{e,t,\text{exp},n}})^2} \quad (3)$$

2.5. Characterization techniques

The morphological structure of the investigated samples was examined using scanning electron microscope (NEO SCOPE JEOL, JCM-5000).

FTIR analysis of the samples was carried out in KBr pellets in the range of 400–4,000 cm^{-1} using a 8400S spectrometer (Shimadzu, Japan) having a standard mid-IR deuterated triglycine sulfate (DTGS) detector.

XRD analyses of adsorbents were carried out with a Miniflex II diffractometer (Rigaku, USA) using $\text{CuK}\alpha$ radiation (1.5406 Å) and a graphite monochromator at room temperature, operated at 30 kV and 15 mA. Diffraction patterns were recorded between 20° and 90° (2 θ) using increments of 0.02° and a counting time of 2 s.

The specific surface area of samples was determined from nitrogen adsorption/desorption isotherms at 77 K, obtained from a Quantachrome type Autosorb IQ device. The specific surface areas were calculated according to the BET method [32].

TGA of the materials was performed on instruments LABSYS_{Sevo} de (SETARAM, France) at a heating rate of 10°C/min from 25°C to 900°C in nitrogen gas.

3. Results and discussion

3.1. Characterization

3.1.1. Scanning electron microscopy

The SEM images of MgAl-CO_3 , MgAlC, PANI and MgAlC-PANI are shown in Fig. 1. Fig. 1(a) shows the SEM micrograph of MgAl-CO_3 before calcination. The surface of MgAl-CO_3 exhibited smooth and tight structure. The image of the MgAlC (Fig. 1(b)) shows clearly distinct shapes, and mineralogical angulate particles of different sizes, whereas the PANI in Fig. 1(c) shows aggregated particles with no uniform size. The surface morphologies of MgAlC-PANI (Fig. 1(d)) were clearly different from those of the MgAlC (Fig. 1(b)) and PANI (Fig. 1(c)).

3.1.2. FTIR analysis

The results of the FTIR studies of MgAl-CO_3 , MgAlC, PANI and MgAlC-PANI are shown in Fig. 2. The FTIR spectrum of the MgAl-CO_3 shows characteristic bands of hydroxalcite. The bands at 3,453 and 1,629 cm^{-1} are attributed, respectively, to the O–H stretching and bending vibrations of hydroxyl groups (Mg/Al–OH or Al–OH) and water molecules [34]. The small and broad band at 3,070 cm^{-1} is attributed to hydroxyl interactions with carbonate ions impurities in the interlayer and is assigned to the bridging mode H_2O [33]. The band at 1,364 cm^{-1} is assigned to a vibrational mode of the CO_3^{2-} anions [34]. The FTIR spectrum of MgAlC shows bands in the region below 850 cm^{-1} , which are assigned to the vibrational modes of Al–O and Mg–O in the resultant material [16]. FTIR spectrum for PANI prepared in HCl presented characteristic bands at 1,570; 1,470; 1,294 and 1,236; 1,118 and 798 cm^{-1} , which correspond to the stretching vibration frequency of C=C in quinoid rings, C=C in benzenoid rings, C–N (stretching in benzenoid ring and stretching in protonic acid doped PANI), N=Q=N (Q-quinoid) and C–H in aromatic rings, respectively [35,36]. The band at 3,448 cm^{-1} was assigned to the N–H stretching vibration [35]. These bands agreed well with those of PANI (emeraldine salt) reported by Wang et al. [37]. After loading MgAlC by PANI, the characteristic spectrum fingerprints of PANI are present in MgAlC-PANI and a noticeable shift in the peaks from 3,448; 1,570; 1,470; 1,294; 789 to 3,441; 1,573; 1,461; 1,295 and 713 cm^{-1} has been occurring and this shift could be attributed to the physical interaction between MgAlC and PANI [35]. The peaks at the range of 400–500 cm^{-1} can be attributed to bending vibration of Mg/Al–O.

3.1.3. XRD analysis

The XRD patterns of MgAl-CO_3 , MgAlC, PANI and MgAlC-PANI are presented in Fig. 3. The MgAl-CO_3 displays a diffraction pattern that corresponds to a well crystalline hydroxalcite phase, with symmetric reflections at 2 θ = 11.7°, 23.4°, 34.7°, 38.8°, 46.3°, 60.7° and 62.1°. These values corresponding to 7.6 Å (d_{003}), 3.8 Å (d_{006}), 2.6 Å (d_{012}), 2.3 Å (d_{015}), 1.9 Å (d_{018}), 1.5 Å (d_{110}) and 1.5 Å (d_{113}), respectively, are in good agreement with those reported by literature [38]. After calcination, the characteristic reflections of MgAl-CO_3 disappeared and the hydroxalcite phase was transformed into an

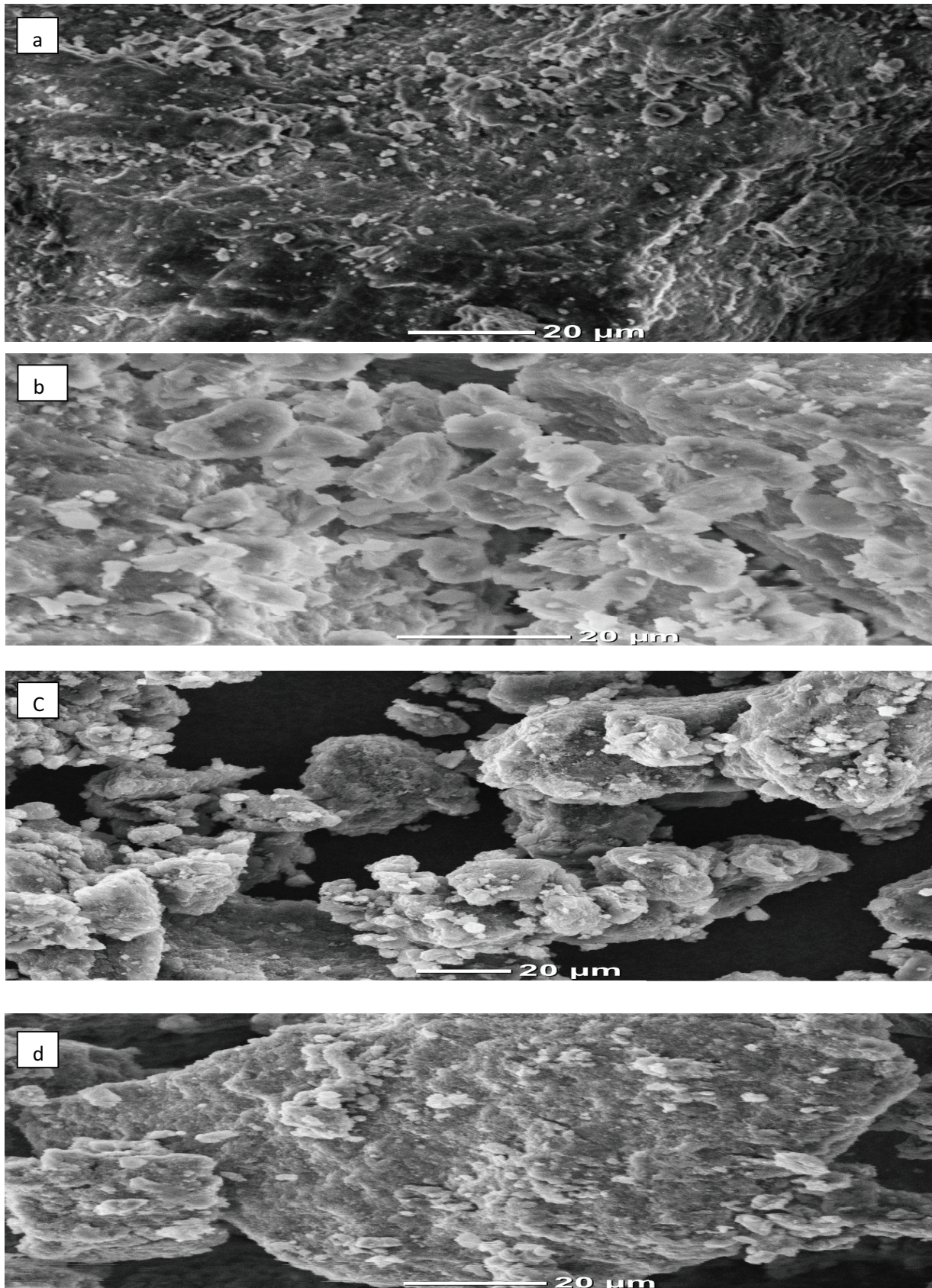


Fig. 1. SEM of MgAl-CO₃ (a), MgAlC (b), PANI (c) and MgAlC-PANI (d).

amorphous structure, due to dehydration and decarbonation according to the modification that appears in Fig. 3. Only a few diffused peaks observed at 43.2° and 62.6° are attributed to mixed oxides [17]. The XRD pattern of PANI shows four peaks centered at $2\theta = 9.1^\circ$, 15.7° , 20.0° and 25.1° . The peaks at $2\theta = 20.0^\circ$ and $2\theta = 25.1^\circ$ may be attributed to periodicity parallel and perpendicular to the polyaniline chain, respectively [39]. The peak at 9.1° may arise from the repeat unit of the polyemeraldine chain [40]. The XRD pattern of the composite MgAlC-PANI shows the same peaks obtained from pure polyaniline, indicating that no additional crystalline order was introduced into the composite [41]. However, reconstruction of the layered structure has not been observed to take place after a chemical oxidation polymerization of aniline on MgAlC by the “memory effect” of CLDHs. This means that the MgAlC particles were dispersed in the polymeric matrix.

3.1.4. BET analysis

Fig. 4 shows the N_2 adsorption–desorption isotherms for MgAl- CO_3 , MgAlC, PANI and MgAlC-PANI. According to the IUPAC classification, the whole samples display the II-type adsorption isotherm characterized by the absence of a plateau in the relative pressure close to 1, evidencing the

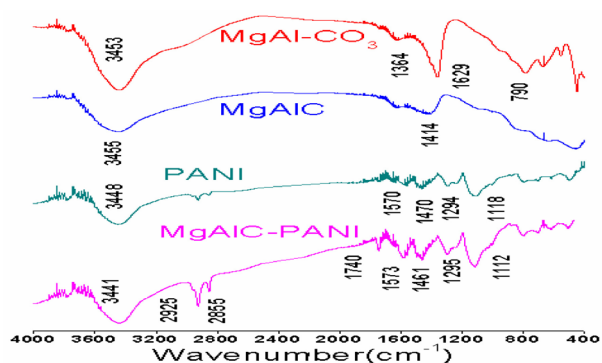


Fig. 2. FTIR spectra of MgAl- CO_3 , MgAlC, PANI and MgAlC-PANI.

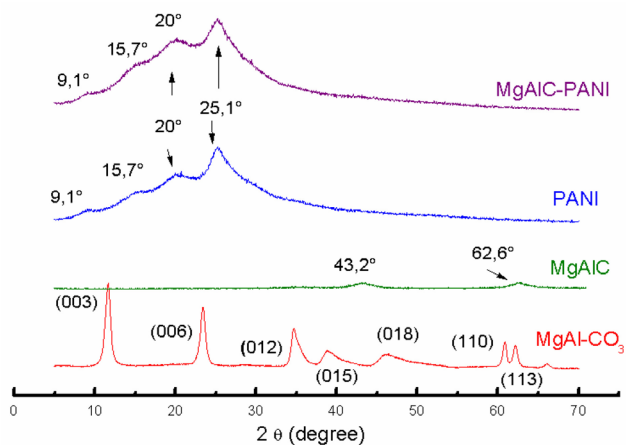


Fig. 3. XRD patterns of MgAl- CO_3 , MgAlC, PANI and MgAlC-PANI.

presence of macropores [42]. However, the hysteresis loop between the adsorption and desorption branches is characteristic of mesoporous materials. Therefore, the presence of both features hints on the coexistence of mesopores and macropores [43]. The specific surface areas of MgAl- CO_3 and MgAlC were 59.0 and 132.0 m^2/g , respectively. The removal of water and carbon dioxide during calcination can lead to the formation of channels and pores [44], which are accessible to the nitrogen molecules and could increase the specific surface area of MgAlC. The total volume (at $P/P_0 = 0.995$) also changed from 0.637 to 0.962 cm^3/g after calcination of the adsorbent MgAl- CO_3 . While the BET surface area of PANI and MgAlC-PANI were 26.5 and 47.8 m^2/g , the volumes obtained were 0.058 and 0.094 cm^3/g , respectively. However, the surface area of the composite MgAlC-PANI was small compared with the parent compound MgAlC. This confirms the successful composite formation of MgAlC with PANI.

3.1.5. TGA analysis

The results of the differential thermogravimetric analysis (Fig. 5) show that the MgAl- CO_3 decomposes according to three steps, the loss of surface water molecules and intercalated ones, from room temperature to $250^\circ C$, is 17% . The second region, (between $250^\circ C$ and $500^\circ C$) where the weight

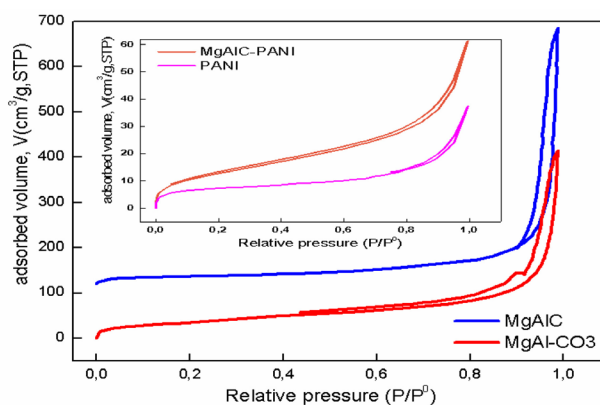


Fig. 4. BET isotherms of the MgAl- CO_3 , MgAlC, PANI and MgAlC-PANI.

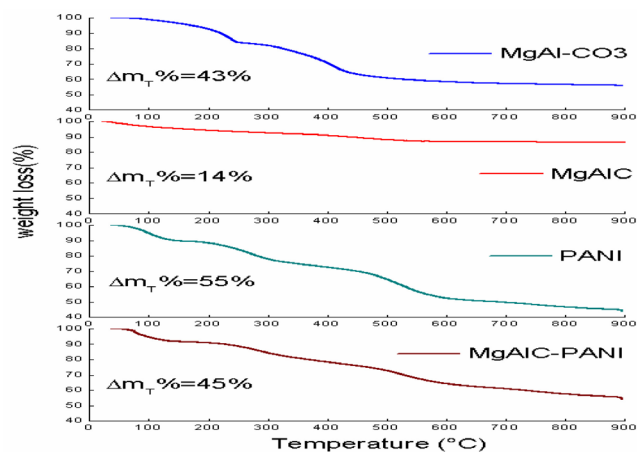


Fig. 5. TG curves of MgAl- CO_3 , MgAlC, PANI and MgAlC-PANI.

loss is 22%, is mainly attributed to the dehydroxylation of the leaves, destruction of the structure and formation of mixed oxides at about 450°C [33,38]. The third step, having an overlap with the second one (mass loss of 4%), is ascribed to the decomposition of CO_3^{2-} anions from the interlamellar space, leading to the collapse of the layered structure concomitantly with the oxide crystallization [33,38]. The TGA curves for the PANI and MgAlC-PANI (Fig. 5) show that MgAlC-PANI undergoes three steps of decomposition similar to those of the pure polyaniline. The first step, from room temperature to approximately 139°C, corresponds to the loss of physisorbed and interlayer water. The weight losses are 9% and 8% for PANI and MgAlC-PANI, respectively. The second weight loss in the temperature range 139°C–355°C is almost 11% and 16% for PANI and MgAlC-PANI, respectively. This loss is due to the thermal dedoping of HCl acid [44]. The third mass loss of about 30% and 25% for PANI and MgAlC-PANI, respectively, occurring beyond 355°C, is attributed to the thermal decomposition and degradation of the PANI chains. The total weight losses of the samples are 43%, 14%, 55% and 45% for MgAl- CO_3 , MgAlC, PANI and MgAlC-PANI, respectively. In addition, the TGA curves of MgAlC, PANI and MgAlC-PANI (Fig. 5) indicated that the amount of pure PANI intercalated on MgAlC-PANI is about 31% ($\Delta m_T\%$ (MgAlC-PANI) – $\Delta m_T\%$ (MgAlC)); 45% – 14% = 31%), lower than that of the pure PANI, which is about 55%.

3.2. Dye adsorption studies

3.2.1. Adsorption isotherms

Adsorption isotherm experiments were carried out to explore the maximum sorption capacity and the distribution of adsorbate between the adsorbent and the liquid phase at equilibrium, which plays a major role in the design of the adsorption system. Fig. 6 shows adsorption isotherms of tartrazine on the different samples. The shape of these isotherms is the H-type according to Giles classification [45]. This isotherm indicates that tartrazine has a high affinity for

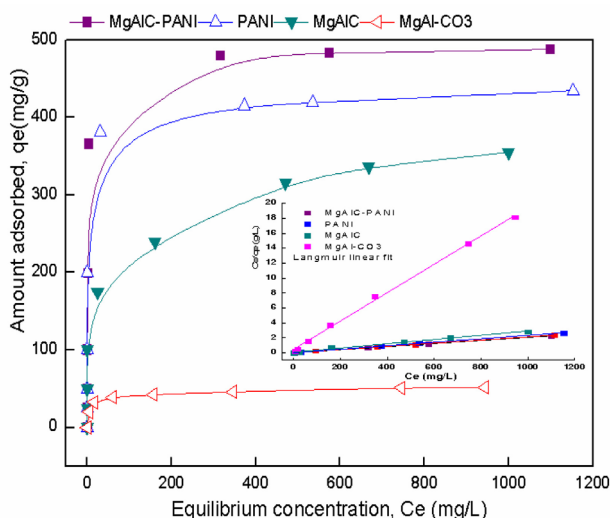


Fig. 6. Equilibrium adsorption data for tartrazine onto MgAl- CO_3 , MgAlC-PANI, PANI and MgAlC.

all adsorbent surfaces, particularly at low concentrations, and represents a system where the dye is strongly attracted by the adsorbent.

In this study, the equations of Langmuir [46] and Freundlich [47] isotherm models are given as follows:

Langmuir isotherm

$$C_e / q_e = C_e / q_{\max} + 1 / (q_{\max} K_L) \quad (4)$$

Freundlich isotherm

$$\ln q_e = \ln K_F + (1/n) \ln C_e \quad (5)$$

where C_e is the equilibrium concentration of tartrazine (mg/L), q_e is the amount of tartrazine adsorbed (mg/g), q_m maximum amount of tartrazine per unit weight of adsorbent (mg/g) for a monolayer coverage and K_L is the Langmuir adsorption equilibrium constant (L/mg) related to the adsorption energy. K_F ($\text{L}^{1/n} \text{mg}^{1-1/n}/\text{g}$) and $1/n$ are the capacity-affinity constant and an exponent in Freundlich isotherm, representing sorption intensity and capacity, respectively.

The values of $0 < 1/n < 1$ indicate favorable adsorption condition.

The Langmuir and Freundlich constants were calculated and their values are given in Table 1. Examining the equilibrium sorption data using above-mentioned adsorption models, it was found that the adsorption of tartrazine followed the Langmuir isotherm. The high values of correlation coefficients ($0.993 \leq R^2 \leq 0.999$) indicate that Langmuir model can be applied to this sorbent system better than Freundlich ($0.641 \leq R^2 \leq 0.992$), revealing the homogeneous nature of the adsorbents and that the adsorption of tartrazine is a monolayer adsorption process. Furthermore, the maximum monolayers of adsorption (q_{\max}) of Langmuir isotherm were 51.6, 352.1, 432.9 and 487.8 mg/g for MgAl- CO_3 , MgAlC, PANI and MgAlC-PANI, respectively.

As MgAlC-PANI is the best adsorbent, only the effect of initial pH of the solution and the kinetics of the MgAlC-PANI will be further studied.

3.2.2. Effect of pH solution on the adsorption of TAR onto MgAlC-PANI

One of the important factors that affect the adsorption is the pH of the dye solution. For this purpose, the pH dependence on the adsorption of tartrazine on MgAlC-PANI was investigated. Fig. 7 shows that the tartrazine removal efficiency slightly changed when the pH values changed from 2 to 9 (about 365 mg/g) and clearly decreased when the pH reached 11 (123 mg/g). The pKa values of different attractor groups representing the tartrazine molecule (sulfonic acid group ($-\text{SO}_3^-$), carboxylate group ($-\text{COO}^-$) and azo group ($-\text{N}=\text{N}-$) were 2.0, 5.0 and 10.9, respectively [48]. Thus, for pH of solution $> \text{pKa}$ ($=2.0$ or 5.0), tartrazine molecules exist in an anionic form and for pH of solution $< \text{pKa}$ ($=2.0$), tartrazine molecules exist in a cationic form [49]. The surface of MgAlC-PANI is also affected by pH. Thus, the emeraldine salt ES form of PANI (under acidic condition), would be positively charged, while the emeraldine base EB form (under alkaline condition), it would be negatively charged

[50]. According to Kuramoto and Genies [51], the transition from the positively charged form (ES) to the negatively charged form (EB) occurs at pH 7–8. In the pH range 2–9, when MgAlC-PANI is added to the solution of tartrazine, the pH of the solution becomes acid (less than 7) and does not change during the adsorption. Therefore, at pH less than 9, the surface of the composites becomes highly positively charged. An electrostatic interaction between negatively charged dye anions with the positively charged adsorbent surface results in a higher adsorption of the dye. At higher pH values, the existence of electrostatic repulsion between the MgAlC-PANI surface and azo-dye anions and the competition between OH⁻ ions and azo dye anions, for the sorption sites cause the decrease in the tartrazine removal efficiency.

3.2.3. Effect of initial dye concentration on the adsorption of TAR onto MgAlC-PANI

To evaluate the effect of initial concentration on removal efficiency and maximum sorption capacity of MgAlC-PANI, it was necessary to generate the equilibrium sorption data at various initial dye concentrations. Experiments were carried out at equilibrium time and the plots of adsorption capacity (q_e) and removal percentage (%) vs. different tartrazine concentrations are shown in Fig. 8. It was found that the removal efficiency of tartrazine dye remains constant (100%) for the initial dye concentration from 25 to 200 mg/L. The percentage sorption decreased (from 92.5% to 29.7%) with increasing tartrazine concentration from 400 to 1,600 mg/L.

3.2.4. Effect of contact time

The suitable contact time between adsorbent and adsorbate is necessary to attain maximum removal of pollutant species. Fig. 9 shows the influence of contact time on the adsorption of tartrazine on MgAlC-PANI with different initial concentrations (50, 100, 200 and 400 mg/L). It was found that for 50, 100 and 200 mg/L, the times taken to reach the equilibrium are 30, 60 and 180 min, respectively. In the case of initial tartrazine concentration of 400 mg/L, the time taken to reach the equilibrium is 1,100 min.

3.2.5. Kinetic model

Many kinetic models have been proposed in the literature. These models are useful for the design and optimization of the effluent-treatment process. In order to investigate the mechanism of TAR adsorption by MgAlC-PANI, the following kinetic models were considered.

3.2.5.1. *Pseudo-first-order kinetic model* The pseudo-first-order kinetic model was proposed by Lagergren [52]. The integrated form of the model is given as follows:

$$\ln(q_e - q_t) = \ln q_e - k_1 \times t \quad (6)$$

where q_e is the amount of dye adsorbed at equilibrium (mg/g), q_t is the amount of dye adsorbed at time t (mg/g), k_1 is the first-order rate constant (min⁻¹) and t is time (min).

A plot of $\ln(q_e - q_t)$ and t will give a linear form, indicating that the adsorption follows first-order kinetics. The values of k_1 and q_e can be determined from the slope and intercept of the

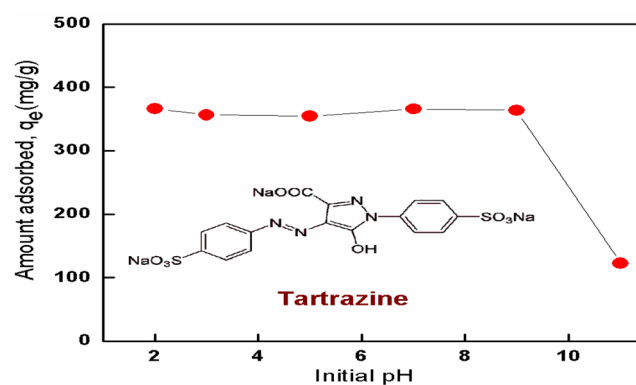


Fig. 7. Effect of the pH for the equilibrium adsorption data of tartrazine on the MgAlC-PANI.

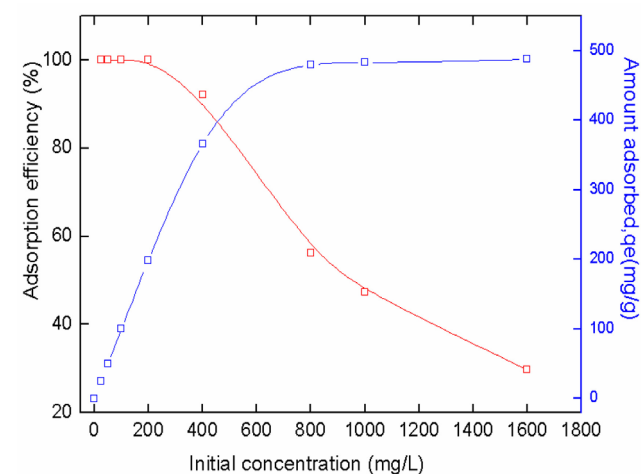


Fig. 8. Effect of initial concentrations on tartrazine removal onto MgAlC-PANI.

Table 1

Isotherm constants for the removal of tartrazine onto MgAl-CO₃, MgAlC, PANI and MgAlC-PANI

| Sample | q_{exp} (mg/g) | Langmuir | | | Freundlich | | |
|----------------------|------------------|------------------|---------------------|-------|-------------------------------------|-------|-------|
| | | q_{max} (mg/g) | $K_L * 10^2$ (L/mg) | R^2 | K_f (mg/g (L/mg) ^{1/n}) | $1/n$ | R^2 |
| MgAlC-PANI | 486.5 | 487.8 | 55.5 | 0.999 | 5.453 | 0.115 | 0.641 |
| PANI | 434.3 | 432.9 | 26.4 | 0.999 | 5.822 | 0.035 | 0.992 |
| MgAlC | 352.6 | 352.1 | 4.5 | 0.993 | 4.508 | 0.198 | 0.990 |
| MgAl-CO ₃ | 51.5 | 52.6 | 4.3 | 0.998 | 2.887 | 0.163 | 0.883 |

plot. The results provided by the pseudo-first-order kinetic plot (figure not shown) at various initial dye concentrations are given in Table 2. The calculated $q_{e,cal}$ and experimental $q_{e,exp}$ values show a large deviation at various initial dye concentrations and the correlation coefficient lies between 0.799 and 0.978. Thus, the Lagergren pseudo-first order rate law failed to explain the adsorption of TAR by MgAlC-PANI with a poor fit at this concentration range.

3.2.5.2. Pseudo-second-order kinetic model The adsorption may also be described by a pseudo-second-order kinetic model [53] if the adsorption does not follow the first order kinetics. The linearized form of the pseudo-second-order model is given as follows:

$$t/q_t = (1/k_2q_e^2) + (1/q_e) \times t \quad (7)$$

where k_2 is the second-order rate constant (g/mg/min). A plot of t/q_t and t should give a linear relationship if the adsorption follows second order, q_e and k_2 can be calculated from the slope and intercept. The pseudo-second-order plot at various initial dye concentrations is given in Fig. 10 and the results are given in Table 2. The equilibrium sorption capacity of q_e (cal) and q_e (exp) is close to each other. According to these results, it is clear that the equilibrium sorption capacity q_e increases with increasing the initial dye concentration. The pseudo-second-order rate constant decreases with increasing the concentration. The high dye concentration can result in a high concentration gradient

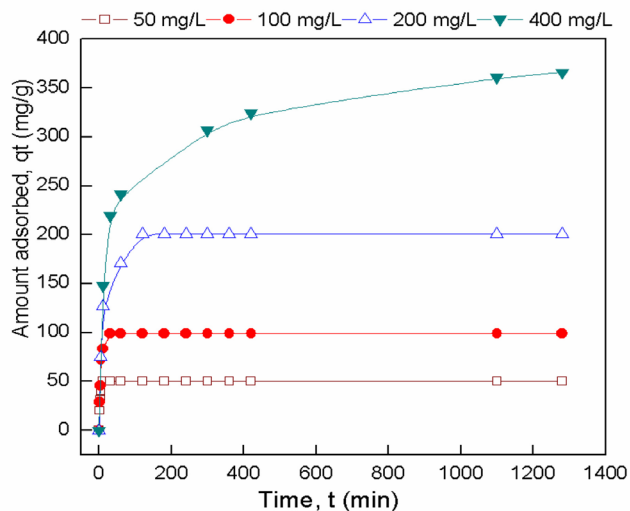


Fig. 9. Kinetic adsorption data for tartrazine onto MgAlC-PANI.

between the solute and the sorbent, thereby the rate of adsorption decreases. The adsorption of TAR by MgAlC-PANI is well explained by the pseudo-second-order kinetics with a very high correlation coefficient $0.998 < R^2 < 1$, which suggests that the adsorption of tartrazine onto MgAlC-PANI follows the pseudo-second-order kinetic model. This supports the assumption, that the rate-determining step may be chemisorption, involving an exchange of electrons between adsorbent and adsorbate. Previous results related to the adsorption kinetics of dye by different polyaniline composites also support the pseudo-second-order model [25–30].

3.2.6. Diffusion mechanism

Kinetic studies can only explain solute–surface interactions during adsorption process but not the diffusion mechanism between solutes and particles. Thus, the kinetic data were further analyzed using Weber–Morris intraparticle diffusion model based on Fick's second law of diffusion [54]. The intraparticle mass transfer diffusion model proposed by Weber and Morris can be described by the equation given below:

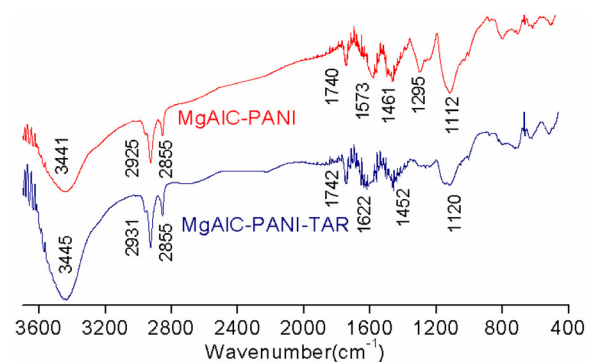
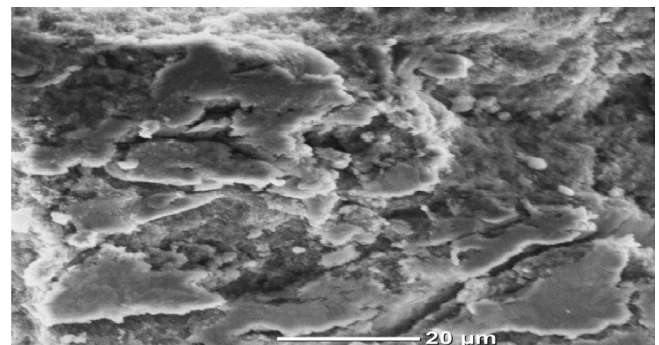


Fig. 10. FTIR and SEM of MgAlC-PANI after tartrazine adsorption.

Table 2
Kinetic parameters for the adsorption of tartrazine onto MgAlC-PANI

| C_0 (mg/L) | q_{exp} | Pseudo-first-order kinetics | | | Pseudo-second-order kinetics | | | Intraparticle diffusion | | |
|--------------|-----------|-----------------------------|--------------------|-------|------------------------------|-------------|-------|----------------------------------|------|-------|
| | | k_1 (min ⁻¹) | $q_{e,cal}$ (mg/g) | R^2 | $k_2 \cdot 10^3$ (g/mg min) | $q_{e,cal}$ | R^2 | k_3 (mg/g min ^{1/2}) | C | R^2 |
| 50 | 50 | 0.032 | 46.1 | 0.978 | 41.2 | 50.2 | 1.000 | 16.4 | 3.74 | 0.998 |
| 100 | 100 | 0.184 | 87.9 | 0.941 | 9.3 | 99.3 | 0.999 | 26.5 | 3.71 | 0.905 |
| 200 | 200 | 0.027 | 144.6 | 0.799 | 1.3 | 202.0 | 0.999 | 14.9 | 58.9 | 0.682 |
| 400 | 366 | 0.003 | 201.3 | 0.942 | 0.075 | 371.7 | 0.998 | 20.3 | 92.0 | 0.834 |

$$q_t = k_3 \sqrt{t} + C \quad (8)$$

where C (mg/g) is the intercept and k_3 (mg [g/min]) is the intraparticle diffusion rate constant, which can be calculated from the slope of the linear plots of q_t vs. $t^{1/2}$. As shown in Table 2, the values of R^2 obtained from the linear regression plots of q_t vs. $t^{1/2}$ (figure not shown) for the whole time data of the sorption process were low. The low R^2 values suggest that the Weber–Morris model could not describe well the experimental data and that the tartrazine adsorption process was not limited by the intraparticle diffusion [36]. The values of k_3 at different initial concentrations were determined from the slopes of the linear portions and included in Table 2.

3.2.7. Suggested mechanism

The adsorption mechanism was investigated by SEM and FTIR analysis. According to the SEM image of the MgAlC-PANI after dye adsorption (Fig. 10), the pores disappeared and the surface was smoothed and altered slightly which further confirms the structural changes in the MgAlC-PANI sample. In the FTIR spectrum of MgAlC-PANI after dye adsorption (Fig. 10), some modifications were verified in relation to the spectrum before adsorption. After the adsorption of TAR onto MgAlC-PANI, many functional groups shifted to different bands. The bands at 3,441; 2,925; 1,740; 1,573; 1,112 transferred to higher frequencies at 3,446; 2,934; 1,742; 1,622 and 1,120 cm^{-1} , respectively, whereas the peak at 1,461 cm^{-1} slightly shifted to a lower frequency band at 1,452 cm^{-1} . On the contrary, the peak at 1,295 cm^{-1} disappeared after adsorption. These changes indicate that the possible interaction of surface sites with TAR ions. From the results mentioned above, it can be concluded that the MgAlC-PANI possessed a high adsorption capacity for the removal of tartrazine and that the adsorbed amount is higher on MgAlC and PANI. The following mechanism suggested that the adsorption of dye onto MgAlC-PANI maybe as follows:

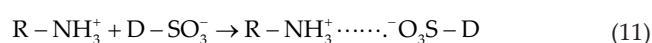
Dyes are first dissolved and their sulphonate groups ($\text{D-SO}_3\text{Na}$) are dissociated and converted to anionic dye ions, according to the equations from (9) to (11).



Also, the amino groups of MgAlC-PANI were protonated in the presence of H^+ .



Due to the electrostatic attraction between these two counter ions, the adsorption process then proceeds,



This interaction mechanism was also verified in other research, which used clay coated by polyaniline as adsorbents [23–29].

3.2.8. Regeneration studies

The low tartrazine adsorption quantity onto MgAlC-PANI at high pH value implies that tartrazine loaded adsorbent can be desorbed in alkaline solution. Therefore, desorption experiment of tartrazine from MgAlC-PANI was performed using NaOH as desorbing agent and HCl solution as the activation agent [55]. Repetitively, the regenerated adsorbents were applied to treat the same concentration of tartrazine solution ($C = 205$ mg/L). The regenerated samples were then used for four consecutive adsorption/desorption cycles. As obvious from Fig. 11, after each cycle, there is a decrease in the adsorption efficiency of the adsorbent with removal percentages evaluated at 100%, 66%, 64% and 57% for the first, second, third and fourth cycle, respectively. This result suggested that the MgAlC-PANI can be reused many times as an adsorbent for wastewater treatment.

3.3. Comparison with other adsorbents

The maximum adsorbed amount of tartrazine on MgAlC-PANI is compared with those other adsorbents. The disadvantage of the adsorbents gathered in Table 3 is the adjustment of pH of the dye wastewater from alkaline to acid. The adsorbent MgAlC-PANI exhibits much higher sorption capacity for tartrazine as compared with other reported adsorbents in Table 3 [56–61] in a wide range of pH.

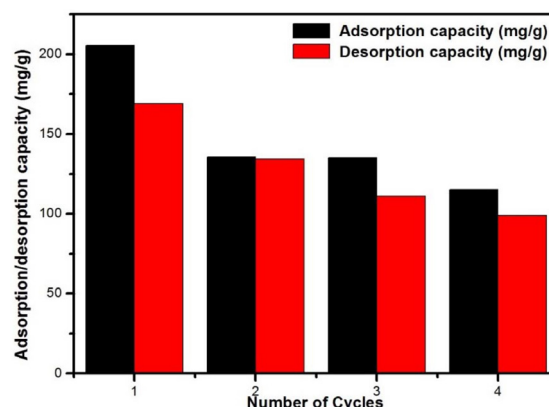


Fig. 11. Removal efficiency of tartrazine by MgAlC-PANI for four regeneration cycles.

Table 3
Comparison of the adsorption capacity of MgAlC-PANI with various adsorbents

| Adsorbents | q_{max} (mg/g) | References |
|---|----------------------------|------------|
| Bottom ash | 12.6 | [56] |
| Deoiled soya | 24.6 | [56] |
| Hen feather | 74.8 | [57] |
| Activated carbon of <i>Lantana camara</i> | 90.9 | [58] |
| Polyaniline nanolayer composite | 2.47 | [59] |
| Cross-linked chitosan-coated bentonite | 294.1 | [60] |
| 5 Ag/CNTs | 84.04 | [49] |
| Polypyrrole-coated tenorite nanoparticle | 42.5 | [61] |
| MgAlC-PANI | 487.8 | This study |

4. Conclusions

In this study, polyaniline/MgAlC composite was synthesized using a chemical oxidation polymerization of aniline in acid medium, in presence of ammonium persulphate as an oxidant. The physico-chemical characterizations have shown that the polyaniline used in the synthesis of MgAlC-PANI composite has been successfully grafted onto MgAlC. The adsorption isotherm of tartrazine onto adsorbents was described using Langmuir and Freundlich isotherm models. However, the Langmuir isotherm model was found to fit better with the experimental data than the Freundlich isotherm model. The maximum adsorption capacity of the adsorbent was measured to be 487.8 mg/g. Initial pH had no significant effect on tartrazine adsorption in the pH range 2–9. The kinetic study indicated that the tartrazine adsorption obeyed pseudo-second-order model. Regeneration tests indicated that MgAlC-PANI could be used repeatedly. These results show that MgAlC-PANI is a promising candidate as an adsorbent for the removal of tartrazine from aqueous solutions.

References

- [1] H.E. Reynel-Avila, D.I. Mendoza-Castillo, A. Bonilla-Petriciolet, Relevance of anionic dye properties on water decolorization performance using bone char: adsorption kinetics, isotherms and breakthrough curves, *J. Mol. Liq.*, 219 (2016) 425–434.
- [2] A.B. Albadarin, M. Charara, B.M. Abu Tarboush, M.N.M. Ahmad, Tonni Agustiono Kurniawan, Mu Naushad, G.M. Walker, C. Mangwandi, Mechanism analysis of tartrazine biosorption onto masau stones; a low cost by-product from semi-arid regions, *J. Mol. Liq.*, 242 (2017) 478–483.
- [3] Sílvia C.R. Santos, Rui A.R. Boaventura, Adsorption of cationic and anionic azo dyes on sepiolite clay: equilibrium and kinetic studies in batch mode, *JECE*, 4 (2016) 1473–1483.
- [4] G. Sharma, Z.A. AlOthman, A. Kumar, Sh. Sharma, S.K. Ponnusamy, M. Naushad, Fabrication and characterization of a nanocomposite hydrogel for combined photocatalytic degradation of a mixture of malachite green and fast green dye, *Nanotechnol. Environ. Eng.*, 2 (2017) 4.
- [5] E. Daneshvar, A. Vazirzadeh, A. Niazi, M. Kousha, Mu. Naushad, A. Bhatnagar, Desorption of Methylene blue dye from brown macroalgae: effects of operating parameters, isotherm study and kinetic modeling, *J. Cleaner Prod.*, 152 (2017) 443–453.
- [6] A.A. Alqadami, Mu. Naushad, M.A. Abdalla, M.R. Khan, Z.A. AlOthman, Adsorptive removal of toxic dye using Fe₃O₄-TSC nanocomposite: equilibrium, kinetic, and thermodynamic studies, *J. Chem. Eng. Data*, 61 (2016) 3806–3813.
- [7] Mu. Naushad, Z.A. AlOthman, Md.R. Awual, S.M. Alfadul, T. Ahmad, Adsorption of rose Bengal dye from aqueous solution by amberlite Ira-938 resin: kinetics, isotherms, and thermodynamic studies, *Desal. Wat. Treat.*, 57 (2016) 13527–13533.
- [8] A. Albadarin, M. Collins, Mu Naushad, S. Shirazian, G. Walker, C. Mangwandi, Activated lignin–chitosan extruded blends for efficient adsorption of methylene blue, *Chem. Eng. J.*, 307 (2017) 264–272.
- [9] G. Sharma, Mu. Naushad, A. Kumar, Sh. Rana, Sh. Sharma, A. Bhatnagar, F.J. Stadler, A.A. Ghfar, M.R. Khan, M.R. Khan, Efficient removal of coomassie brilliant blue R-250 dye using starch/ poly(alginate-chitosan) nanohydrogel, *Process Saf. Environ. Prot.*, 109 (2017) 301–310.
- [10] S.C.R. Santos, R.A.R. Boaventura, Adsorption of cationic and anionic azo dyes on sepiolite clay: Equilibrium and kinetic studies in batch mode, *JECE*, 4 (2016) 1473–1483.
- [11] M.A. Kamboh, A.A. Bhatti, I.B. Solangi, S.T.H. Sherazi, S. Memon, Adsorption of direct black-38 azo dye on p-tert-butylcalixarene immobilized material, *ARAB J. CHEM.*, 7 (2014) 125–131.
- [12] L. Wang, Application of activated carbon derived from 'waste' bamboo culms for the adsorption of azo dyes: kinetic, equilibrium, and thermodynamic studies, *J. Environ. Manage.*, 102 (2012) 79–87.
- [13] A.B. Volikov, S.A. Ponomarenko, A.I. Konstantinov, K. Hatfield, I.V. Perminova, Nature-like solution for removal of direct brown 1 azo dye from aqueous phase using humics-modified silica gel, *Chemosphere*, 145 (2016) 83–88.
- [14] L. Zheng, C. Wang, Y. Shu, X. Yan, L. Li, Utilization of diatomite/chitosan-Fe (III) composite for the removal of anionic azo dyes from wastewater: equilibrium, kinetics and thermodynamics, *Colloids Surf., A*, 468 (2015) 129–139.
- [15] H. Wang, Q. Yang, C.H. Niu, I. Badea, Adsorption of azo dye onto nanodiamond surface, *Diamond Relat. Mater.*, 26 (2012) 1–6.
- [16] H. Zaghouane-Boudiaf, M. Boutahala, L. Arab, Removal of methyl orange from aqueous solution by uncalcined and calcined MgNiAl Layered double hydroxides (LDHs), *J. Chem. Eng.*, 187 (2012) 142–149.
- [17] D. Chebli, A. Bouguettoucha, A. Reffas, C. Tiar, M. Boutahala, H. Gulyas, A. Amrane, Removal of the anionic dye Biebrich scarlet from water by adsorption onto calcined and non-calcined Mg–Al layered double hydroxides, *Desal. Wat. Treat.*, 57 (2016) 1–13.
- [18] W.T. Reichle, Synthesis of anionic clay minerals (mixed metal hydroxides hydrotalcite), *Solid State Ionics*, 22 (1986) 135–141.
- [19] D. Carriazo, del. M. Arco, C. Martin, V. Rives, A comparative study between chloride and calcined carbonate hydrotalcites as adsorbents for Cr(VI), *Appl. Clay Sci.*, 37 (2007) 231–239.
- [20] C. Geng, T. Xu, Y. Li, Z. Chang, X. Sun, X. Lei, Effect of synthesis method on selective adsorption of thiosulfate by calcined Mg–Al layered double hydroxides, *J. Chem. Eng.*, 232 (2013) 510–518.
- [21] F.R. Zhu, L. Zhang, J.L. Zeng, L. Zhu, Z. Zhu, X.Y. Zhu, R.H. Li, Z.H. Xiao, Z. Cao, Preparation and thermal properties of palmitic acid/polyaniline/ copper nanowires form-stable phase change materials, *J. Therm. Anal. Calorim.*, 115 (2014) 1133–1141.
- [22] C. Xu, H. Chen, F. Jiang, Adsorption of perfluorooctane sulfonate (PFOS) and perfluorooctanoate (PFOA) on polyaniline nanotubes, *Colloids Surf., A*, 479 (2015) 60–67.
- [23] E. Gençec, Color removal from anaerobic/aerobic treatment effluent of bakery yeast wastewater by polyaniline/beidellite composite materials, *JECE*, 3 (2015) 2484–2491.
- [24] M. Milojevic-Rakić, A. Janošević, J. Krstić, B.N. Vasiljević, V. Dondur, G. Ćirić-Marjanovic, Polyaniline and its composites with zeolite ZSM-5 for efficient removal of glyphosate from aqueous solution, *Microporous Mesoporous Mater.*, 180 (2013) 141–155.
- [25] J. Wang, X. Han, H. Maa, Y. Ji, L. Bi, Adsorptive removal of humic acid from aqueous solution on polyaniline/attapulgit composite, *Chem. Eng. J.*, 173 (2011) 171–177.
- [26] H. Cui, Y. Qian, Q. Li, Q. Zhang, J. Zhai, Adsorption of aqueous Hg(II) by a polyaniline/attapulgit composite, 211–212 (2012) 216–223.
- [27] S. Karthikaikumar, M. Karthikeyan, K.K. Satheesh, Removal of Congo Red dye from aqueous solution by polyaniline-montmorillonite composite, *Chem. Sci. Rev. Lett.*, 2 (2014) 606–614.
- [28] J. Chen, X. Hong, Y. Zhao, Y. Xia, D. Li, Q. Zhang, Preparation of flake-like polyaniline/montmorillonite nanocomposites and their application for removal of Cr(VI) ions in aqueous solution, *J. Mater. Sci.*, 48 (2013) 7708–7717.
- [29] Y. Kong, J. Wei, Z. Wang, T. Sun, C. Yao, Z. Chen, Heavy metals removal from solution by polyaniline/palygorskite composite, *J. Appl. Polym. Sci.*, 22 (2011) 2054–2059.
- [30] H. Javadian, M.T. Angaji, M. Naushad, Synthesis and characterization of polyaniline/γ-alumina nanocomposite: a comparative study for the adsorption of three different anionic dyes, *J. Ind. Eng. Chem.*, 20 (2014) 3890–3900.
- [31] C. Sun, B. Xiong, Y. Pan, H. Cui, Adsorption removal of tannic acid from aqueous solution by polyaniline: analysis of operating parameters and mechanism, *J. Colloid Interface Sci.*, 487 (2017) 175–181.
- [32] S. Brunauer, P.H. Emmett, E. Teller, Adsorption of gases in multimolecular layers, *J. Am. Chem. Soc.*, 60 (1938) 309–319.

- [33] S. Özgümüş, M.K. Gök, A. Bal, G. Güçlü, Study on novel exfoliated polyampholyte nanocomposite hydrogels based on acrylic monomers and Mg–Al–Cl layered double hydroxide: synthesis and characterization, *Chem. Eng. J.*, 223 (2013) 277–286.
- [34] H. Zaghoulane-Boudiaf, M. Boutahala, C. Tiar, L. Arab, F. Garin, Treatment of 2,4,5-trichlorophenol by MgAl–SDBS organo-layered double hydroxides: kinetic and equilibrium studies, *Chem. Eng. J.*, 173 (2011) 36–41.
- [35] A. Olad, F.F. Azhar, A study on the adsorption of chromium (VI) from aqueous solutions on the alginate-montmorillonite/polyaniline nanocomposite, *Desal. Wat. Treat.*, 52 (2013) 1–12.
- [36] R. Karthik, S. Meenakshi, Synthesis, characterization and Cr(VI) uptake study of polyaniline coated chitin, *Int. J. Biol. Macromol.*, 72 (2015) 235–242.
- [37] J. Wang, K. Zhang, L. Zhao, Sono-assisted synthesis of nanostructured polyaniline for adsorption of aqueous Cr (VI): effect of protonic acids, *Chem. Eng. J.*, 239 (2014) 123–131.
- [38] F. Cavani, F. Trifiro, A. Vaccari, Hydrotalcite-type anionic clays: preparation, properties and applications, *Catal. Today*, 11 (1991) 173–301.
- [39] J. Zhao, Z. Qin, T. Li, Z. Li, Z. Zhou, M. Zhu, Influence of acetone on nanostructure and electrochemical properties of interfacial synthesized polyaniline nanofibers, *Proc. Nat. Sci. Mater.*, 25 (2015) 316–322.
- [40] L. Zhang, Y. Long, Z. Chen, M. Wan, The effect of hydrogen bonding on self-assembled polyaniline nanostructures, *Adv. Funct. Mater.*, 14 (2004) 693–698.
- [41] C.M. Chang, C.J. Weng, C.M. Chien, T.L. Chuang, T.Y. Lee, J.M. Yeh, Y. Weib, Polyaniline/carbon nanotube nanocomposite electrodes with biomimetic hierarchical structure for Supercapacitors, *J. Mater. Chem. A*, 1 (2013) 4719–4722.
- [42] M.A. Alves-Rosa, L. Martins, P. Hammer, S.H. Pulcinelli, C.V. Santilli, Sulfated zirconia foams synthesized by integrative route combining surfactants, air bubbles and sol-gel transition applied to heterogeneous catalysis, *RSC Adv.*, 8 (2016) 6686–6694.
- [43] Z. Yu, D. Chen, M. Ronning, V. Torbjorn, E. Ochoa-Fernandez, A. Holmen, Large scale synthesis of carbon nanofibers on Ni–Fe–Al hydrotalcite derived catalysts. I. Preparation and characterization of the Ni–Fe–Al hydrotalcites and their derived catalysts, *Appl. Catal. A*, 338 (2008) 136–146.
- [44] M.A. Salem, R.G. Elsharkawy, M.F. Hablas, Adsorption of Brilliant Green dye by polyaniline/silver nanocomposite: kinetic, equilibrium, and thermodynamic studies, *Eur. Polym. J.*, 75 (2016) 577–590.
- [45] C.H. Giles, T.H. Mac Ewan, S.N. Nakhwa, D. Smith, Studies in adsorption. Part XI. A system of classification of solution adsorption isotherms and its use in diagnosis of adsorption mechanisms and in measurement of specific surface areas of solids, *J. Chem. Soc.*, 111 (1960) 3973–3993.
- [46] I. Langmuir, The constitution and fundamental properties of solids and liquids, *J. Am. Chem. Soc.*, 38 (1916) 2221–2295.
- [47] H.M.F. Freundlich, Über die adsorption in loesungen, *Z. Phys. Chem.*, 57 (1906) 385–470.
- [48] C. Klett, A. Barry, I. Balti, P. Lelli, F. Schoenstein, N. Jouini, Nickel doped zinc oxide as a potential sorbent for decolorization of specific dyes, methylorange and tartrazine by adsorption process, *J. Environ. Chem. Eng.*, 2 (2014) 914–926.
- [49] J. Goscianska, R. Pietrzak, Removal of tartrazine from aqueous solution by carbon nanotubes decorated with silver nanoparticles, *Catal. Today*, 249 (2015) 259–264.
- [50] K. Haitham, S. Razak, M.A. Nawi, Kinetics and isotherm studies of methyl orange adsorption by a highly recyclable immobilized polyaniline on a glass plate, *Arabian J. Chem.*, (2018). <https://doi.org/10.1016/j.arabjc.2014.10.010>.
- [51] N. Kuramoto, E.M. Geniès, Micellar chemical polymerization of aniline, *Synth. Met.*, 68 (1995) 191–194.
- [52] S.Y. Lagergren, Zurtheorie der sogenannten adsorption gelösterstoffe (On the theory of so-called adsorption of solutes), *K. Sven. Vetensk.akad Handl.*, 24 (1898) 1–39.
- [53] Y.S. Ho, G. McKay, Pseudo-second-order model for sorption processes, *Process Biochem.*, 34 (1999) 451–465.
- [54] W.J. Weber, J.C. Morris, Kinetics of adsorption on carbon from solution, *J. Sanit. Eng. Div., ASCE*, 89 (1963) 31–60.
- [55] N. Wang, J. Li, W. Lv, J. Feng, W. Yan, Synthesis of polyaniline/TiO₂ composite with excellent adsorption performance on acid red G, *RSC Adv.*, 5 (2015) 21132–21141.
- [56] A. Mittal, J. Mittal, L. Kurup, Adsorption isotherms, kinetics and column operations for the removal of hazardous dye, Tartrazine from aqueous solutions using waste materials—Bottom Ash and De-Oiled Soya, as adsorbents, *J. Hazard. Mater.*, 136 (2006) 567–578.
- [57] A. Mittal, L. Kurup, J. Mittal, Freundlich and Langmuir adsorption isotherms and kinetic for the removal of tartrazine from aqueous solutions using hen feathers, *J. Hazard. Mater.*, 146 (2007) 243–248.
- [58] R.K. Gautam, P.K. Gautam, S. Banerjee, V. Rawat, S. Soni, S.K. Sharma, M.C. Chattopadhyaya, Removal of Tartrazine by activated carbon biosorbents of *Lantana camara*: kinetics, equilibrium modeling and spectroscopic analysis, *JECE*, 3 (2015) 79–88.
- [59] R. Ansari, M.B. Keivani, A.F. Delavar, Application of polyaniline nanolayer composite for removal of tartrazine dye from aqueous solutions, *J. Polym. Res.*, 18 (2011) 1931–1939.
- [60] W.S.W. Ngah, N.F.M. Ariff, M.A.K.M. Hanafiah, Preparation, characterization and environmental application of crosslinked chitosan-coated bentonite for tartrazine adsorption from aqueous solutions, *Water Air Soil Pollut.*, 206 (2010) 225–236.
- [61] V. Srivastava, P. Maydannik, Y.C. Sharma, M. Sillanpää, Synthesis and application of polypyrrole coated tenorite nanoparticles (PPy@TN) for the removal of the anionic food dye ‘tartrazine’ and divalent metallic ions viz. Pb(II), Cd(II), Zn(II), Co(II), Mn(II) from synthetic wastewater, *RSC Adv.*, 5 (2015) 80829–80843.